# Improved Hybrid Reactive Power Compensation System Based on FC and STATCOM and Its Control Method*

*Xiheng Liang*[1], *Fei Jiang*[1*], *Xing Peng*[1], *Liansong Xiong*[2], *Yongbin Jiang*[3], *Samir Gautam*[4] *and Zhichang Li*[5]

(1. School of Electrical and Information Engineering,
Changsha University of Science & Technology, Changsha 410076, China;
2. School of Electrical Engineering, Xi'an Jiaotong University, Xi'an 710049, China;
3. School of Electrical and Electronic Engineering,
Nanyang Technological University, Singapore 639798, Singapore;
4. School of Electrical Engineering, The University of Sydney, Sydney NSW 2006, Australia;
5. Beijing Sgitg-Accenture Information Technology Co., Ltd., Beijing 100080, China)

**Abstract**: The purpose of this study is to solve the main problems in distribution networks, including increased line loss and reduced power supply quality caused by insufficient capacitive reactive power. To reduce the capacity, voltage, and current stress of an active module of a compensation device and improve the cost performance of the device, an improved hybrid reactive power compensation system based on a fixed capacitor (FC) and a static synchronous compensator (STATCOM) is proposed. The topological structure and basic operating principle of the proposed reactive power compensation system are introduced. In addition, from the perspectives of output voltage, current, power, loss of the active part, and system compensation cost, the performances of the proposed reactive compensator and the inductively coupled STATCOM (L-STATCOM) are compared and analyzed. Furthermore, the key parameters of the proposed system are designed, and the joint optimization control strategy of the FC and STATCOM is studied. The correctness and effectiveness of the proposed topology structure and control method are verified by simulations.

**Keywords**: Static synchronous compensator, hybrid topology, reactive power compensation, fixed capacitor

## 1 Introduction

With the definition of carbon peaking and neutrality goals and the in-depth progress of the construction of new power systems, the power grid has played a more prominent role as a hub platform for energy conversion, utilization, and transmission configuration [1-3]. In recent years, with the continuous development of the power grid system, inductive loads, such as electric motors and electric arc furnaces, have increased sharply, so the demand for capacitive reactive power in a distribution network is also increasing. If the phenomenon of capacitive reactive power shortage exists in a distribution network for a long time, it not only increases the line loss and reduces the power factor of the system but also reduces the power supply quality of the grid, and it can even endanger the stability of the power system [4-7].

At present, reactive power compensation technology, as one of the important applications of power electronics technology, has an important role in power system operation. Therefore, it has been widely studied, and various types of reactive power compensation device have been proposed. Among them, a shunt capacitor is an example of early reactive power compensation technology. It has a simple

Manuscript received January 28, 2022; revised March 25, 2022; accepted May 10, 2022. Date of publication June 30, 2022; date of current version June 6, 2022.

* Corresponding Author, E-mail: jiamg85521@126.com

* Supported by the General Project of Hunan Natural Science Foundation (2021JJ30715), the Scientific Research Fund of Hunan Provincial Education Department (20B029) and the Graduate Research Innovation Project of Changsha University of Science & Technology (CX2021SS52).
Digital Object Identifier: 10.23919/CJEE.2022.000012

structure and can improve the voltage quality and reduce the power loss. A thyristor switched capacitor (TSC) can effectively reduce the impulse current when the capacitor bank is mechanically switched. However, the mentioned compensation technologies can only achieve graded compensation but cannot continuously adjust the reactive power, and, generally, overcompensation or undercompensation occurs [8-9]. To compensate for that the inability of the shunt capacitor and TSC to achieve continuous compensation, a thyristor controlled reactor (TCR) and a fixed capacitor (FC) or a TSC and a TCR can be used together. In such a combination, a TCR controls the current flowing through the reactor to provide reactive power continuously by adjusting the trigger angle of a thyristor. However, the adjusting TCR generates harmonics, and the compensation range of the two devices is limited [10-11]. With the development of power electronics technology, a static synchronous compensator (STATCOM) has been proposed. The STATCOM represents an advanced and continuously adjustable static reactive power compensation device. However, the STATCOM has certain disadvantages, such as high DC-link voltage, large capacitance, and high cost [12-15]. Therefore, how to achieve continuous but economical compensation for high-capacity reactive power has become a leading research topic in the field of electrical engineering.

Considering the compensation effect and cost, some hybrid reactive power compensation devices with superior performance have emerged. Their topology is mainly composed of active modules and passive devices connected in series or parallel.

Hybrid parallel structures: A hybrid topology composed of the STATCOM and static var compensator (SVC) connected in parallel has been introduced [16-19]. In this topology, the SVC of the passive part of the device compensates for most of the capacitive reactive power and reduces the output capacity of the STATCOM. However, the coordinated control of the active and passive parts is complex, and the DC-link voltage on the active part is high. A capacitive coupling STATCOM (C-STATCOM) was connected in parallel with thyristor-controlled series compensation (TCSC) [20]. Although this device can expand the range of reactive power compensation and lower the DC-link voltage, harmonics are injected into the power grid, so additional filtering devices are required.

Hybrid series structures: A C-STATCOM composed of capacitors and a traditional STATCOM connected in series has been proposed [21-23]. To improve the range of reactive power compensation, the TSC and TCSC modules have been replaced by the coupling capacitance [24-25]. To solve the problem of the low utilization rate of hybrid equipment, a series structure of a thyristor-controlled LC filter (TCLC) and a STATCOM was introduced [26]. This structure can achieve reactive power compensation, and it has arc suppression capabilities. The four devices can reduce the output voltage of the active part by using the series capacitor, TSC, TCSC, and TCLC, which in turn reduces the output capacity and DC-link voltage of the STATCOM. However, the output current of the active part of the four devices is larger, and the current stress brought by the switching device and the total cost of the device are high.

To address the shortcomings of the existing solutions, an improved hybrid reactive power compensation system based on the FC and STATCOM is proposed. It was developed by using an idea of the hybrid series-parallel type and considering that an FC composed of multiple capacitors connected in series or parallel.

The remainder of this article is organized as follows. In Section 2, the topological structure of the proposed reactive power compensation system is introduced, and its basic working principle is explained. The performance advantages of the proposed reactive power compensation system are analyzed in Section 3. The key circuit parameters of the proposed system are discussed in Section 4. The control strategy of the joint optimization of the FC and STATCOM is studied in Section 5. The correctness and feasibility of the proposed topology and control strategy are verified by simulation, as described in Section 6. Finally, conclusions are drawn in Section 7.

## 2 Topology and operating principle

### 2.1 Circuit topology

The circuit topology of the proposed reactive power

compensator is shown in Fig. 1, which shows that it includes a DC-link capacitor $C_{dc}$, a voltage source inverter (VSI), an output filter inductor $L_f$, and a fixed capacitor $C$. The fixed capacitor $C$ is composed of capacitors $C_1$ and $C_2$ connected in series. The VSI is placed between capacitors $C_1$ and $C_2$ and connected to them through a filter inductor $L_f$.

Compared with the traditional L-STATCOM structure [27], the proposed compensator structure includes a parallel connection of capacitor $C_2$ and the AC output side of the VSI and a serial connection of capacitor $C_1$ and the grid-connected branch. Capacitor $C_1$ can withstand the main fundamental voltage drop, thereby reducing the AC output voltage and DC-link voltage of the VSI. Furthermore, capacitor $C_2$ can reduce the output current of the VSI through the shunt action, thereby reducing the current stress of the insulated gate bipolar transistor (IGBT) in the VSI.

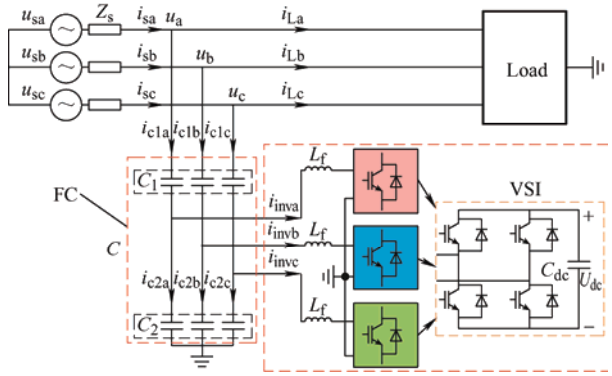


Fig. 1 Topology of the proposed reactive power compensator

In Fig. 1, $u_{sa}$, $u_{sb}$, and $u_{sc}$ represent the phase voltages of the power supply on the grid side, $i_{sa}$, $i_{sb}$, and $i_{sc}$ represent the phase currents on the grid side, $Z_s$ represents the system line impedance, $u_a$, $u_b$, and $u_c$ denote the voltages of the proposed reactive power compensator access point, $i_{La}$, $i_{Lb}$, and $i_{Lc}$ are the three-phase resistive-inductive load currents, $i_{c1a}$, $i_{c1b}$, and $i_{c1c}$ represent the three-phase currents flowing into capacitor $C_1$ at the grid connection point, $i_{c2a}$, $i_{c2b}$, and $i_{c2c}$ represent the three-phase currents flowing into capacitor $C_2$, and $i_{inva}$, $i_{invb}$, and $i_{invc}$ are three-phase fundamental currents from the VSI output.

## 2.2 Operating principle

For the proposed reactive power compensator topology shown in Fig. 1, an equivalent single-phase fundamental wave operating circuit can be obtained, as shown in Fig. 2. In Fig. 2, arrows indicate positive directions of voltage and current, $U$ is the voltage of the compensator junction point, $U_{C1}$ and $I_{C1}$ represent the voltage and current of capacitor $C_1$, respectively, $U_{C2}$ and $I_{C2}$ represent the voltage and current of capacitor $C_2$, respectively, $U_{Lf}$ is the voltage of a filter inductor $L_f$, and $U_{inv}$ and $I_{inv}$ denote the output voltage and current of the VSI, respectively.

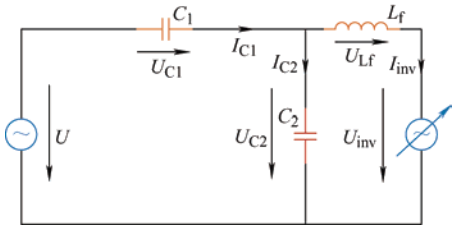


Fig. 2 Equivalent single-phase circuit of the proposed reactive power compensator

Ignoring the inductive reactive power, the reactive power transmitted to the power grid by the proposed reactive compensator can be calculated by

$$Q_c = Q_{C1} + Q_{C2} + Q_m[(-1)^{\lambda} m] \tag{1}$$

where $Q_{C1} = U_{C1}^2/(1/\omega C_1)$, $Q_{C2} = U_{C2}^2/(1/\omega C_2)$, $Q_{C1}$ and $Q_{C2}$ represent the output reactive powers of the capacitors $C_1$ and $C_2$, respectively, $Q_m$ is the maximum output reactive power capacity of the VSI, and $m$ is in the range of [0, 1].

When the capacitor $C$ is in the undercompensated state, then $\lambda$=0. When the capacitor $C$ is under full compensation, then $m$=0. When the capacitor $C$ is in the overcompensated state, then $\lambda$=1.

As shown in Fig. 3, when capacitors $C_1$ and $C_2$ compensate for most of the reactive load power, they are in the undercompensated state, and the VSI needs to output residual capacitive reactive power. When capacitors $C_1$ and $C_2$ compensate for all the reactive load power, achieving the full-compensation state, the VSI does not need to provide additional capacitive reactive power, and its output current is approximately zero. When the reactive power compensated for by capacitors $C_1$ and $C_2$ is larger than the reactive load power, it is in the overcompensated state, and the VSI must output an appropriate inductive reactive power to absorb the capacitive reactive power overcompensated for by the capacitor. In the three described

compensation situations, the VSI and capacitors $C_1$ and $C_2$ coordinate and cooperate to achieve the reactive load power compensation.

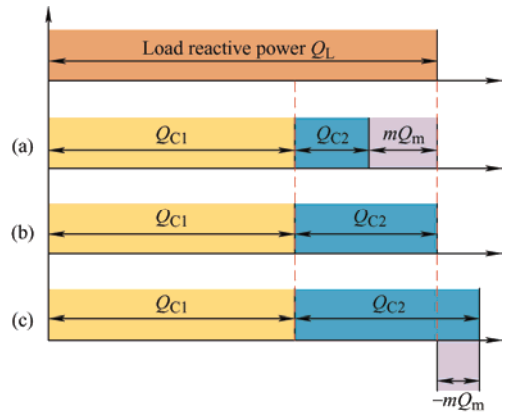


Fig. 3 VSI output capacity changes when the fixed capacitor is under (a) partial compensation, (b) full compensation, and (c) overcompensation

## 3 Performance analysis

### 3.1 VSI output voltage

The operating vector diagrams of the traditional L-STATCOM system and the proposed reactive power compensation system are shown in Figs. 4a and 4b, respectively. From the diagrams in Fig. 4, the voltage equations of the two systems can be expressed as

$$u = i_{inv}(j\omega L_f) + u_{inv} = u_{Lf} + u_{inv} \tag{2}$$

$$u = u_{c2} + u_{c1} = i_{inv}(j\omega L_f) + u_{inv} + u_{c1} = u_{Lf} + u_{inv} + u_{c1} \tag{3}$$

where $u$ is the voltage of the compensator joint point, $u_{Lf}$ is the output filter inductor voltage, $i_{inv}$ and $u_{inv}$ are the output AC current and voltage of the VSI, respectively, and $i_{c1}$, $i_{c2}$, $u_{c1}$, and $u_{c2}$ are the currents and voltages of capacitors $C_1$ and $C_2$ in the proposed system, respectively.

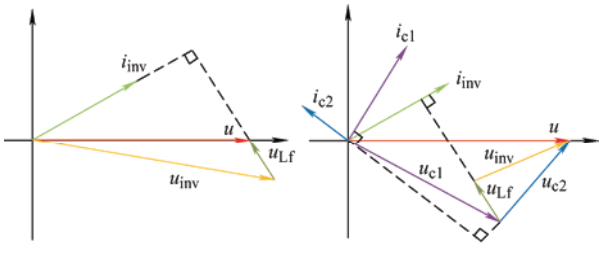


(a) L-STATCOM (b) Proposed system

Fig. 4 Operating vector diagrams

When the output current of the VSI is equal, since the voltage of capacitor $C_1$ ($u_{c1}$) is added to the right side of Eq. (3), the output AC voltage of the VSI ($u_{inv}$) can be reduced. In addition, because $u_{inv}$ is related to the DC-link voltage, increasing the capacitance of capacitor $C_1$ can reduce the DC-link voltage $U_{dc}$.

### 3.2 VSI output current

The reactive current vector diagrams of the L-STATCOM system and the proposed one are shown in Figs. 5a and 5b, respectively. Because both systems mainly realize full compensation for the reactive current of the load, the active components of the output current in the compensation process can be ignored in the analysis. According to the diagrams in Fig. 5, the reactive current equations of the two systems can be expressed by

$$I_{Lq} = -I_{invq} \tag{4}$$

$$I_{Lq} = -I_{c1q} = -(I_{invq} + I_{c2q}) \tag{5}$$

where $I_{Lq}$ and $I_{invq}$ denote the reactive current of the load and the output reactive current of the VSI, respectively, and $I_{c1q}$ and $I_{c2q}$ are the reactive currents flowing through capacitors $C_1$ and $C_2$ in the proposed system, respectively.

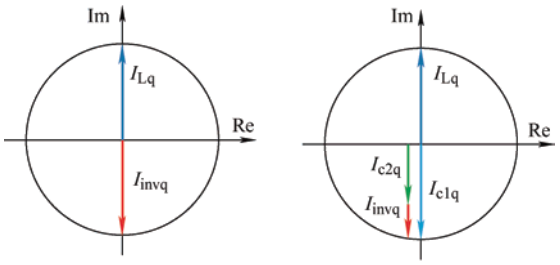


(a) L-STATCOM (b) Proposed system

Fig. 5 Reactive current vector diagrams

When the reactive load power is constant (i.e., the reactive current is unchanged), because the reactive current of capacitor $C_2$ ($I_{c2q}$) is added to the right side of Eq. (5), an increase in the capacitance of capacitor $C_2$ can reduce the output fundamental reactive current of the VSI ($i_{invq}$), which can reduce the output current of the VSI. Thus, the output current of the active part of the proposed compensation system is smaller than that of the L-STATCOM.

### 3.3 VSI output capacity

The output reactive power value of each part of the L-STATCOM system and the proposed system during the reactive power compensation process is shown in Fig. 6. Ignoring the reactive power generated by $L_f$, according to the power balance law, the relationships between the output reactive power capacities of the parts of the two systems are given by

$$Q_L = -Q_{inv} \tag{6}$$

$$Q_L = -(Q_{c1} + Q_{c2} + Q_{inv}) \tag{7}$$

where $Q_L$ and $Q_{inv}$ denote the reactive power of the load and the output reactive power of the VSI, respectively.

In the case of constant reactive load power, because the reactive powers $Q_{c1}$ and $Q_{c2}$ generated by capacitors $C_1$ and $C_2$ are added to the right side of Eq. (7), the addition of capacitors $C_1$ and $C_2$ can reduce the reactive output capacity of the VSI, $Q_{inv}$.

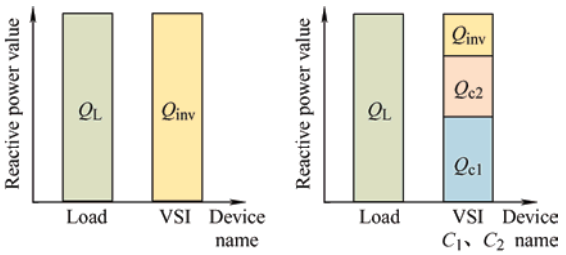


(a) L-STATCOM (b) Proposed system

Fig. 6 Output reactive power value of each part of the two systems

### 3.4 Power loss

The active power loss is mainly composed of the switching loss of the VSI and the loss of the filter reactor. The switching loss includes the turn-on and turn-off losses of a switching device. Assuming that the switching device of the VSI is an IGBT, the switching loss, filter reactor loss, and the total system power loss can be expressed by [28]

$$\begin{cases} P_{IGBT\_loss} = \dfrac{f_s}{T}\displaystyle\int_0^T \left[E_{on}(t) + E_{off}(t)\right] \mathrm{d}t = \\ \qquad\qquad \dfrac{1}{T}\displaystyle\sum_{i=1}^{Tf_s}\left[E_{on}(t_i) + E_{off}(t_i)\right] \mathrm{d}t \\ P_{LAC\_loss} = |I_{inv}|^2 R_f \\ P_{system\_tot} = 6 \times P_{IGBT\_loss} + 3 \times P_{LAC\_loss} \end{cases} \tag{8}$$

where

$$\begin{cases} E_{on} = \dfrac{U_{dc}}{U_{test}} \dfrac{E_{on}(R_{gon})}{E_{on}(R_{gon\_test})} E_{on\_test} \\ E_{off} = \dfrac{U_{dc}}{U_{test}} \dfrac{E_{off}(R_{goff})}{E_{off}(R_{goff\_test})} E_{off\_test} \end{cases} \tag{9}$$

Here, $P_{IGBT\_loss}$, $P_{LAC\_loss}$, and $P_{syetem\_tot}$ represent the switching loss of the IGBT, filter reactor loss, and total system power loss, respectively, $f_s$ is the switching frequency, $T$ denotes the modulation wave period, $R_f$ is the equivalent resistance of the filter reactance, $E_{on}$ and $E_{off}$ represent the energy consumptions of a single pulse in the on and off states of the IGBT, respectively, $E_{on\_test}$ and $E_{off\_test}$ represent the energy consumptions of the single pulse in the on and off states of the IGBT during the product test, respectively, $R_{gon\_test}$ and $R_{goff\_test}$ indicate the on and off resistances of the IGBT gate during the product test, respectively, $R_{gon}$ and $R_{goff}$ represent the on and off gate resistances in actual use, respectively, $E_{on}(R_{gon\_test})$ and $E_{off}(R_{goff\_test})$ represent the on and off energy consumptions corresponding to the gate resistance under the rated current of the IGBT during the product test, respectively, $E_{on}(R_{gon})$ and $E_{off}(R_{goff})$ represent the on and off energy consumptions corresponding to the gate resistance under the actual rated current, respectively, $U_{test}$ is the $U_{CE}$ test value of the IGBT, $U_{dc}$ is the DC-link voltage, and $E_{on}(t_i)$ and $E_{off}(t_i)$ represent the on and off energy consumptions of the switching device of the IGBT at time $t_i$, respectively. The values of $E_{on}$, $E_{off}$, and other parameters can be obtained from the IGBT module specification information.

For instance, if a 1 200 V/400 A IGBT switch tube of the FF400R12KE3 model under the Infineon brand is used, then $R_{gon}$=$R_{goff}$=1.8 Ω, $U_{test}$=600 V, $E_{on}$=17 mJ, $E_{off}$=42 mJ, and $R_f$=0.2 Ω. According to these parameters and Eqs. (8) and (9), the total power loss of the system can be obtained, as shown in Fig. 7. Fig. 7 reveals that the system power loss is positively related to both the DC-link voltage and the output current of the VSI. When the DC-link voltage and the output current of the VSI increase, the system loss also increases. Because the DC-link voltage and the output current of the VSI of the proposed system are smaller than those of the L-STATCOM, the power loss of the proposed system is less compared with the L-STATCOM power loss.

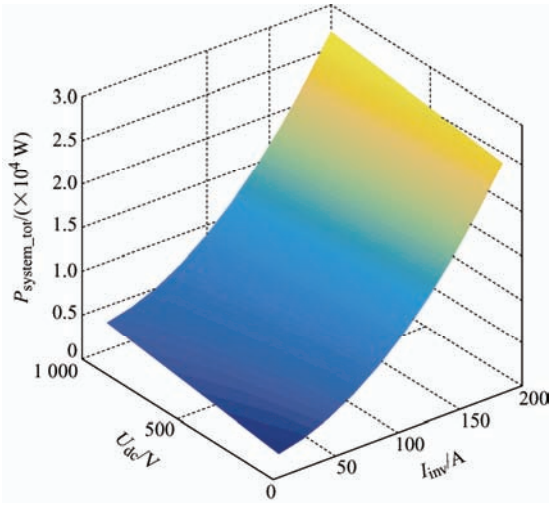


Fig. 7 System power loss diagram

### 3.5 Compensation cost

The system compensation cost mainly consists of the costs of the active and passive parts, which can be expressed as follows

$$Cost = Cost_{\text{Active}} + Cost_{\text{Passive}} = Cost_{\text{IGBT}} + Cost_{\text{DC\_Cap}} + Cost_{\text{Passive}} \quad (10)$$

where $Cost$ denotes the total cost of system compensation, $Cost_{\text{Active}}$ is the cost of the active part, $Cost_{\text{Passive}}$ is the cost of the passive part, $Cost_{\text{IGBT}}$ is the cost of the IGBT, and $Cost_{\text{DC\_Cap}}$ is the cost of the VSI DC-link capacitor.

The IGBT of the VSI in the L-STATCOM requires high voltage- and current-resistant levels, and its DC side requires a large capacitance, so the overall cost of the reactive power compensation of the L-STATCOM increase significantly. Compared with the L-STATCOM, although the passive part (i.e., fixed capacitance $C$) is added to the proposed system, the output voltage, current, capacity, and DC-link voltage of the VSI are significantly reduced; thus, the DC capacitance, voltage-resistant level, and current-resistant level of the IGBT are reduced accordingly. And under the same voltage level, the capacitance cost is much less than that of the IGBT. Therefore, the total cost of the reactive power compensation of the proposed system is reduced compared with the L-STATCOM.

To illustrate the advantages of the proposed compensator, it is compared with hybrid reactive power compensation devices proposed previously [18, 21], as shown in Fig. 8. One of the previously proposed topologies realizes reactive power compensation through a parallel connection of the SVC and STATCOM [18]. The SVC compensates for most of the reactive power and reduces the output current and reactive capacity of the active part. However, this topology has the problems of high DC-link voltage, inverter loss, and cost. In the other previously introduced topology [21], the series capacitor can effectively reduce the output active capacity and DC-link voltage so that the power loss of the VSI and the compensation cost are reduced. However, the problem of a large VSI output current still exists. A comprehensive comparison shows that the proposed system combines the advantages of the previously proposed topologies [18, 21]. In the proposed system, the series capacitor decreases the output active capacity and DC-link voltage, and the parallel capacitor decreases the output current of the VSI so that its loss and cost are reduced.

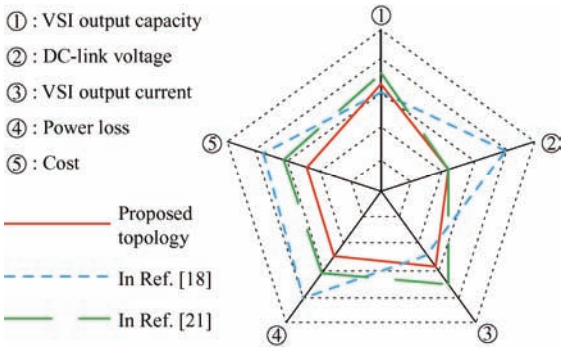


Fig. 8 Performance comparison diagram of different structures

## 4 System parameter setting

To give the proposed compensator its full compensation ability and improve its reliability, it is necessary to set the key parameters of the proposed circuit reasonably and properly. The parameters to be considered include filter inductance $L_f$, DC-link voltage $U_{dc}$, and fixed capacitance $C$ (i.e., the resulting capacitance of capacitors $C_1$ and $C_2$ connected in series). These parameters are analyzed in detail in the following.

According to Fig. 2, the output impedance of the proposed reactive power compensation system is a second-order link, which has a series resonance point. Voltage $U$ can be regarded as a disturbance whose

effect on the output current can be ignored; thus, in this study, the output voltage $U_{inv}$ is used as a control input, and the output current $I_{inv}$ is used as a control output. According to the state space equation, transfer function of the input-output can be obtained as follows [24].

$$G(s)=\frac{I_{inv}(s)}{U_{inv}(s)}=\frac{(C_1+C_2)s}{L_f(C_1+C_2)s^2+1} \tag{11}$$

To facilitate parameter analysis and design, the simulation values of filter inductance $L_f$ and capacitances of capacitors $C_1$ and $C_2$ are substituted into Eq. (11), and the amplitude-frequency curve of the transfer function $G(s)$ is obtained, as shown in Fig. 9. According to the results in Fig. 9, there is a resonance peak in the output impedance of the system, and the resonance angular frequency can be calculated by $\omega_r=1/\sqrt{L_f(C_1+C_2)}$. If the series resonance occurs at the fundamental frequency, the gain at the resonant frequency suddenly increases, so the fundamental current component increases sharply. This affects the IGBT of the VSI and system stability. Therefore, when selecting the values of $L_f$ and capacitances $C_1$ and $C_2$, it is necessary to pay attention to whether the series resonance occurs.

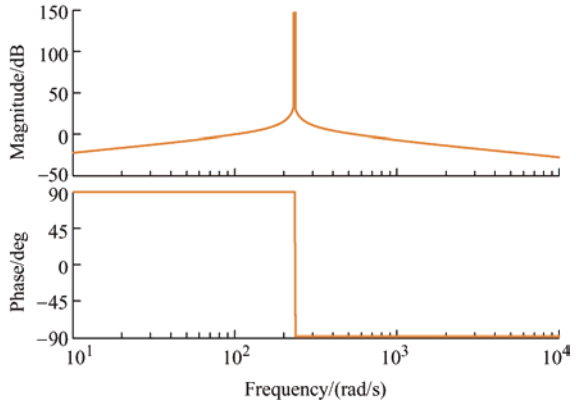


Fig. 9 Bode diagram of transfer function $G(s)$

### 4.1 Filter inductance $L_f$

According to the general selection principle of the traditional DSTATCOM, the output filter inductance $L_f$ of the VSI can be calculated by

$$L_f=\frac{U_s^2X^*}{\omega Q_N} \tag{12}$$

where $U_s$ is the grid voltage, $Q_N$ is the rated reactive power, $\omega$ is the fundamental angular frequency of the grid, $X^*$ is the reactance ratio, and its value range is [0.15, 0.3].

### 4.2 Series and parallel capacitors

Considering the requirements of actual application scenarios, the rated reactive power of the load is set to $Q_N$, and its reactive power fluctuation range is set to $\pm Q_f$. The series and parallel capacitors must match each other, and the constraints can be defined as

$$\begin{cases} C=\dfrac{Q_N+Q_f}{\omega[\omega L_f(Q_N+Q_f)+U_s^2]} \\ C=\dfrac{C_1\cdot C_2}{C_1+C_2} \\ C_2\approx 3C_1 \\ C_1>C \\ C_2>C \\ \omega<\dfrac{1}{\sqrt{L_fC}}<\omega_s \end{cases} \tag{13}$$

where $\omega_s$ is the angular frequency of the VSI switch.

To avoid fundamental wave series resonance between $L_f$ and capacitances $C_1$ and $C_2$, the value of the angular frequency must satisfy the following condition

$$\omega\neq 1/\sqrt{L_f(C_1+C_2)} \tag{14}$$

The capacitance values of capacitors $C_1$ and $C_2$ can be obtained by Eqs. (13) and (14).

### 4.3 DC-link voltage

To ensure the normal operation of the proposed compensator in the reactive load power range, the DC-link voltage constraints of the VSI are defined as

$$\begin{cases} M\leqslant\dfrac{2}{\sqrt{3}}=1.154\,7 \\ \dfrac{MU_{dc}}{2}-U_{sm}\geqslant U_\Delta \end{cases} \tag{15}$$

where $M$ denotes the amplitude modulation ratio of the VSI, which is set to the maximum value of 1.154 7, and $U_{sm}$ is the phase voltage amplitude of the VSI grid-connected point.

Based on Eq. (15), the DC-link voltage should satisfy the following condition

$$U_{dc}\geqslant\frac{2(U_{sm}+U_\Delta)}{1.154\,7} \tag{16}$$

To achieve a better compensation effect, the value of $U_\Delta$ in Eq. (16) cannot be zero. Because the

presented deduction process utilizes the minimum value, the final DC-link voltage reference value also must have an appropriate margin.

## 5 Control strategy

A block diagram of the control strategy of the proposed reactive power compensation system is shown in Fig. 10. It includes two main parts: the reference current calculation and the VSI control. In this study, the focus was on the reactive power compensation, and the capacitor voltage balance control on the DC side of the VSI was not analyzed, so this content is not included in the control block diagram.

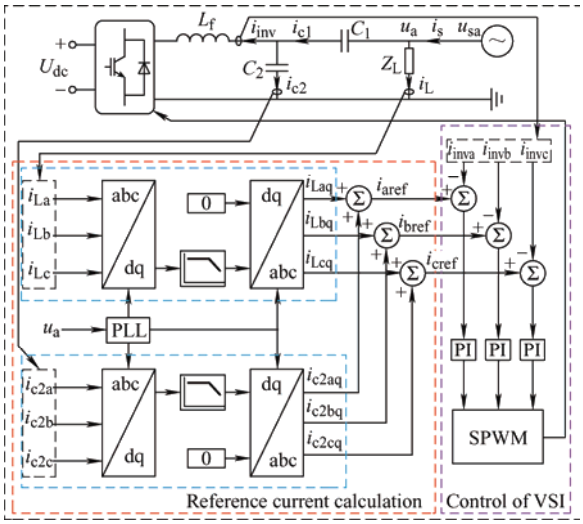


Fig. 10 Control block diagram of the proposed system

First, the three-phase load currents $i_{La}$, $i_{Lb}$, and $i_{Lc}$ are used to obtain reactive and active current components (i.e., $i_{Lq}$ and $i_{Ld}$) through Parker transformation. Similarly, the three-phase current of capacitor $C_2$ is transformed to obtain $i_{c2q}$ and $i_{c2d}$. Second, channels $i_{Ld}$ and $i_{c2d}$ are eliminated and set to zero. Meanwhile, the DC components of the reactive power components $i_{Lq}$ and $i_{c2q}$ are obtained by a low-pass filter. Third, the load's reactive current components $i_{Laq}$, $i_{Lbq}$, and $i_{Lcq}$ and the reactive current components of capacitor $C_2$, $i_{c2aq}$, $i_{c2bq}$, and $i_{c2cq}$ can be obtained by inverse Parker transformation of the DC components. Then, the reactive power components of the two currents are combined to obtain command signals $i_{aref}$, $i_{bref}$, and $i_{cref}$. Finally, the output currents $i_{inva}$, $i_{invb}$, and $i_{invc}$ of the VSI are subtracted from the command current signal to obtain the error signals. The error signals are passed through the proportional-integral regulator (PI) to obtain the modulated wave and then compared with the triangular carrier to generate the driving pulse of the VSI.

## 6 Simulation results

To verify the effectiveness and feasibility of the proposed structure and the control method of the proposed reactive power compensation system, a simulation model of a 0.4 kV power distribution system connected to the compensation system was built using Matlab/Simulink software. The simulation system parameters are shown in Tab. 1. The DC-link voltage of the VSI was provided by the ideal DC voltage source.

**Tab. 1 Simulation parameters**

| Parameter | Value | |
|---|---|---|
| | L-STATCOM | Proposed system |
| Grid voltage $U_s$/V | 380 | 380 |
| DC-link voltage $U_{dc}$/V | 800 | 300 |
| Filter inductance $L_f$/mH | 2.3 | 2.3 |
| Single-phase reactive load power $P_L$/kVar | 20 | 20 |
| Single-phase active load power $Q_L$/kW | 20 | 20 |
| Capacitance $C_1$/mF | — | 2 |
| Capacitance $C_2$/mF | — | 6 |

### 6.1 Comparative analysis of system performance

Under the condition of consistent system parameters, the reactive power compensation effects of the L-STATCOM and the proposed reactive power compensator in static compensation were compared.

During the simulation, the L-STATCOM and the proposed compensator were set to be input at 0.1 s. A performance comparison of the two systems is shown in Fig. 11. The phase-space waveform diagrams of the output A-phase voltage and current of the VSI are presented in Figs. 11a and 11b, respectively, where $u_L$, $u_N$, $i_L$, and $i_N$ represent the moduli of the VSI output voltage and current (i.e., the amplitude of the instantaneous voltage and current), $R$ represents the radius of the circle, and parameter sets ($u_{L\_\alpha}$, $u_{L\_\beta}$, $i_{L\_\alpha}$, $i_{L\_\beta}$) and ($u_{N\_\alpha}$, $u_{N\_\beta}$, $i_{N\_\alpha}$, $i_{N\_\beta}$) represent the voltage and current values in the $\alpha\beta$ two-phase stationary coordinate system, respectively. The total harmonic distortion (THD) curves of the A-phase output current

of the VSI and its three-phase reactive power in the two systems are presented in Figs. 11c and 11d, respectively.

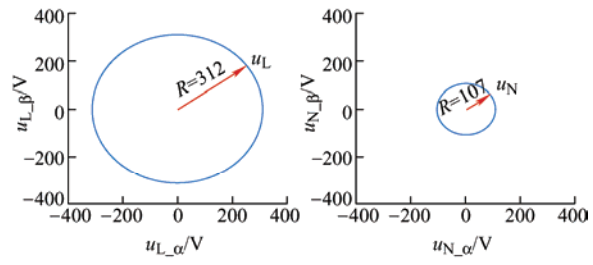


(a) Phase-space waveform diagram of the output A-phase voltage of the VSI

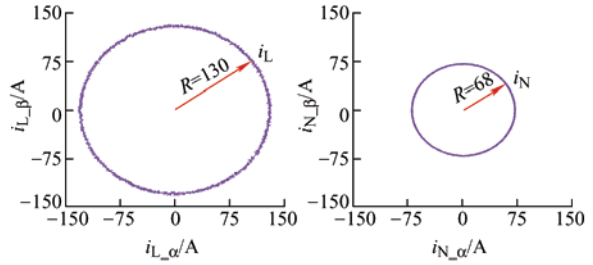


(b) Phase-space waveform diagram of the output A-phase current of the VSI

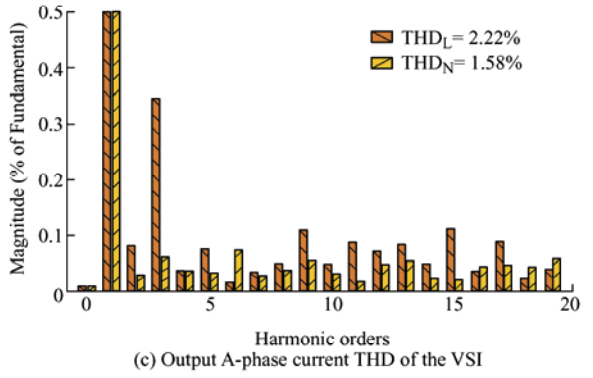


(c) Output A-phase current THD of the VSI

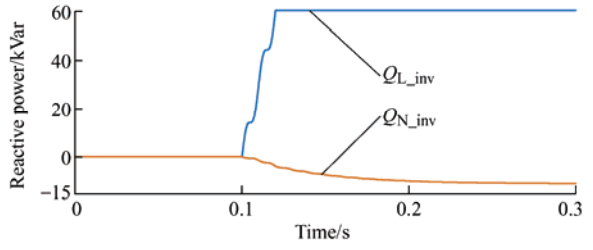


(d) Output three-phase reactive power of the VSI

Fig. 11 Performance comparison of the L-STATCOM and the proposed reactive power compensator

As shown in Fig. 11, when the three-phase load inductive reactive power of 60 kVar was compensated for, the amplitude of the fundamental voltage output by the VSI in the proposed reactive power compensation system was 107 V, the amplitude of the fundamental current was 68 A, and the current THD was 1.58%. At this time, the compensation state of the fixed capacitor was overcompensated, and the three-phase inductive reactive power output by the VSI was 10 kVar. In the L-STATCOM system, the amplitude of the fundamental voltage output by the VSI was 312 V, the amplitude of the fundamental current was 130 A, and the current THD was 2.22%. The three-phase capacitive reactive power output by the VSI was 60 kVar. Compared with the L-STATCOM, the output fundamental voltage, current, and capacity of the VSI in the proposed reactive power compensation system were reduced by 66%, 48%, and 83%, respectively. Meanwhile, the THD of the VSI compensation current was also reduced, as shown in Tab. 2. The results show that the output voltage, current, and reactive capacity of the VSI could be reduced, and the current compensation quality could be improved by reasonably setting the capacitance of the series-parallel capacitor in the proposed reactive power compensator.

**Tab. 2 Performance analysis**

| VSI | L-STATCOM | Proposed topology | Improvements achieved by proposed structure |
|---|---|---|---|
| Output voltage amplitude/V | 312 | 107 | Reduced by 66% |
| Output current amplitude/A | 130 | 68 | Reduced by 48% |
| Output reactive power/kVar | 60 | 10 | Reduced by 83% |
| Current THD(%) | 2.22 | 1.58 | — |
| DC-link voltage/V | 800 | 300 | — |

The reactive power compensation effects of the L-STATCOM and the proposed reactive power compensator are shown in Fig. 12, where $U_{Lsa}$, $U_{Nsa}$, $I_{Lsa}$, and $I_{Nsa}$ represent the A-phase voltages and currents on the grid side of the two systems, respectively. Before the compensator was put into operation, because of the resistive inductive load, the voltage phase on the grid side was ahead of the current phase, and the values of the active and reactive powers of the load were the same during this period; thus, the power factor of the two systems was 0.707. The reactive power compensation effect of the L-STATCOM is shown in Fig. 12a, which shows that, after the system reached stability, the voltage phase on the grid side was consistent with the current phase, and the power factor increased to one. The reactive power

compensation effect of the proposed reactive power compensator is shown in Fig. 12b. The proposed system became stable after 10 ms. The voltage and current on the grid side were in the same phase, and the power factor increased to one. The results show that the proposed compensator has an excellent reactive power compensation effect as L-STATCOM.

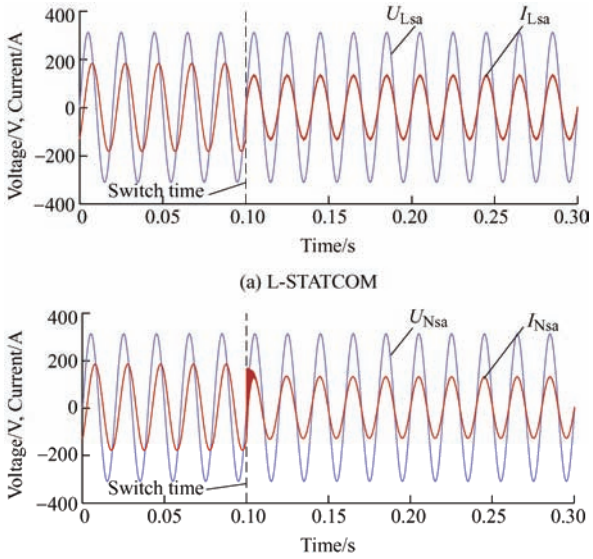


Fig. 12 Reactive power compensation effects

### 6.2 Dynamic compensation analysis

To verify that the proposed reactive power compensator can dynamically compensate for an inductive load with large fluctuations, the simulation conditions were set so that the three-phase resistive inductive load could suddenly increase the reactive power of 10 kVar and active power of 10 kW at 0.3 s and decrease the reactive power of 15 kVar and active power of 15 kW at 0.6 s.

The output A-phase voltage and current of the VSI and capacitors $C_1$ and $C_2$, as well as their respective three-phase compensation reactive power values, are shown in Fig. 13. According to Figs. 13a-13c, during the compensation period of 0.3-0.6 s, when the reactive load power suddenly increased, the current of capacitor $C_1$ also increased, as given by Eq. (5), so its voltage increased accordingly. When the voltage of capacitor $C_1$ increased, according to Eq. (3), the voltage of capacitor $C_2$ and the output voltage of the AC side of the VSI decreased accordingly. Following Ohm's law, the current of capacitor $C_2$ decreased. As shown in Fig. 13d, during this period, capacitors $C_1$ and $C_2$ could compensate for most of the reactive power and were in the undercompensated state. The VSI only needed to provide a small part of the reactive power, and its output current was significantly reduced.

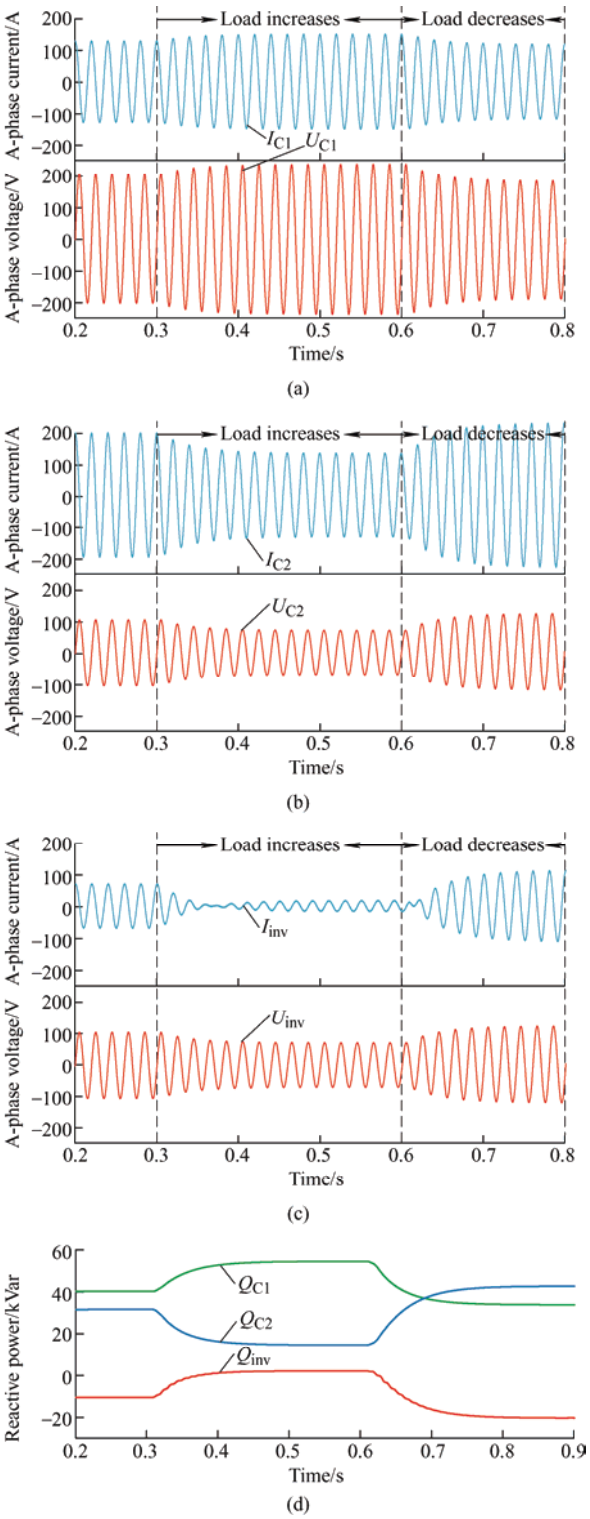


Fig. 13 Output A-phase voltage and current of the VSI and capacitors $C_1$ and $C_2$ and their respective three-phase compensation reactive powers

As shown in Figs. 13a-13c, during the compensation period of 0.6-0.9 s, when the reactive

load power suddenly decreased, the current of capacitor $C_1$ also decreased, according to Eq. (5), so its voltage decreased. When the voltage of capacitor $C_1$ decreased, according to Eq. (3), the voltage of capacitor $C_2$ and the output voltage of the AC side of the VSI increased accordingly. Furthermore, according to Ohm's law, the current of capacitor $C_2$ increased. As shown in Fig. 13d, the sum of the capacitive reactive powers compensated for by capacitors $C_1$ and $C_2$ exceeded the inductive reactive power of the load. In addition, the compensation state of the capacitor was overcompensated during this period, while the VSI needed to modulate inversely and output a part of the inductive reactive power to absorb excess capacitive reactive power, so its output current increased significantly. The VSI and capacitors $C_1$ and $C_2$ cooperated to achieve dynamic compensation of the reactive load power.

The A-phase output current tracking waveform of the VSI and dynamic compensation effect waveform of the proposed system are presented in Fig. 14. In Fig. 14a, $I_{ref\_a}$ and $I_{inv\_a}$ denote the reference A-phase current and the actual output compensation current of the VSI, respectively.

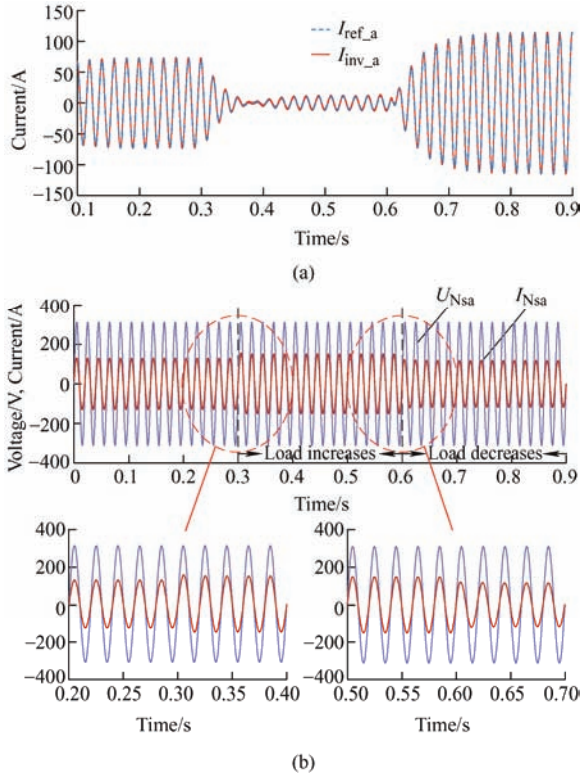


Fig. 14 Output A-phase current tracking waveform of the VSI and dynamic compensation effect waveform of the proposed system

As shown in Fig. 14a, when the reactive load power changed significantly, the current compensated for by the VSI in the proposed reactive power compensator could track the reference current. In addition, Fig. 14b shows that, during the sudden increases in the reactive load power in the intervals of 0.3-0.6 s and 0.6-0.9 s, after the real-time dynamic compensation by the proposed reactive power compensator, the proposed system could reach stability within 10 ms. Moreover, the voltage phase at the grid side was consistent with the current phase, and the power factor increased to one. The above shows that the proposed reactive power compensator can achieve a good dynamic compensation effect.

## 7 Conclusions

An improved hybrid reactive power compensation structure based on the FC and STATCOM was presented, along with its control method. The proposed structure includes a parallel connection of capacitor $C_2$ and the AC output side of the VSI, and a serial connection of capacitor $C_1$ and its grid-connected branch. Capacitors $C_1$ and $C_2$ are connected in series, forming a fixed-capacitance capacitor $C$. The proposed structure has the following advantages. First, capacitor $C_1$ can withstand the main fundamental voltage drop, thereby reducing the AC output voltage and DC-link voltage of the VSI. Second, capacitor $C_2$ reduces the output current of the VSI through the shunt action, thus reducing the current stress of the IGBT in the VSI, which is beneficial for the selection of IGBT devices. The proposed structure can reduce the system compensation cost, active power loss, and output capacity of the VSI. The proposed structure was verified by Matlab/Simulink platform simulations. The simulation results demonstrate the excellent reactive power compensation performance of the proposed structure.

## References

[1] N Ding, J Pan, J Liu, et al. An optimization method for energy structures based on life cycle assessment and its application to the power grid in China. *Journal of Environmental Management*, 2019, 238: 18-24.

[2] J Zhang, C Cheng, S Yu, et al. Sharing hydropower flexibility in interconnected power systems: A case study

for the China Southern Power Grid. *Applied Energy*, 2021, 288(1): 116645.

[3] J Deng, F Jiang, W Wang, et al. Low-carbon optimized operation of integrated energy system considering electric heating flexible load and hydrogen energy refined modeling. *Power System Technology*, 2022, 46(5): 1692-1704.

[4] D Kumar, F Zare. Harmonic analysis of grid connected power electronic systems in low voltage distribution networks. *IEEE J. Emerg. Sel. Topics Power Electron*., 2016, 4(4): 70-79.

[5] D Wu, Y Che, W Li, et al. Optimal allocation of comprehensive resources for large-scale access of electric kiln to the distribution network. *Energy Engineering*, 2021, 118(5): 1549-1564.

[6] N R Tummuru, M K Mishra, S Sriniva. Multifunctional VSC controlled microgrid using instantaneous symmetrical components theory. *IEEE Trans. Sustain. Energy*, 2014, 5(1): 313-322.

[7] T John, C Patsios, D Greenwood. Non-local harmonic current and reactive power compensation for a multi-microgrid system using a series-shunt network device. *IET Gener. Transm. Dis*., 2020, 14(23): 5655-5666.

[8] M M Aman, G B Jasmon, A Bakar, et al. Optimum shunt capacitor placement in distribution system—A review and comparative study. *Renewable & Sustainable Energy Reviews*, 2014, 30: 429-439.

[9] T E Mehdi, V Behrooz. Electric arc furnace power quality improvement by applying a new digital and predicted-based TSC control. *Turkish Journal of Electrical Engineering and Computer Sciences*, 2016, 24: 3724-3740.

[10] S Das, D C hatterjee, S K Goswami. Tuned-TSC based SVC for reactive power compensation and harmonic reduction in unbalanced distribution system. *IET Gener. Transm. Dis*., 2017, 12(3): 571-585.

[11] A Karami-Horestani, M Golshan, H Hajian-Hoseinabadi. Reliability modeling of TCR-FC type SVC using Markov process. *International Journal of Electrical Power & Energy Systems*, 2014, 55: 305-311.

[12] R Xu, Y Yu, R Yang, et al. A novel control method for transformerless H-bridge cascaded STATCOM with star configuration. *IEEE Trans. Power Electron*., 2015, 30(3): 1189-1202.

[13] S Song, S Hwang, G Jang, et al. Improved coordinated control strategy for hybrid STATCOM using required reactive power estimation method. *IEEE Access*, 2019, 7: 84506-84515.

[14] D Wang, X Yuan. Interaction analysis between induction motor loads and STATCOM in weak grid using induction machine model. *Journal of Modern Power Systems and Clean Energy*, 2018, 6(1): 158-167.

[15] Y O Lee, Y Han, C C Chung, et al. Stabilisation of asymmetrically structured back-to-back static synchronous compensator system with non-linear damping control. *IET Power. Electr.*, 2015, 8(10): 1952-1962.

[16] Z Shuai, W Zhu, L An, et al. A dynamic hybrid var compensator and a two-level collaborative optimization compensation method. *IEEE Trans. Power Electron*., 2009, 24(9): 2091-2100.

[17] D Wang, T Wei, W Wu, et al. Low cost hybrid reactive power compensator using coordination control strategies. *IET Gener. Transm. Dis*., 2016, 10(8): 1805-1814.

[18] M T Esfahani, B Vahidi. Development of optimal shunt hybrid compensator based on improving the measurement of various signals. *Measurement*, 2015, 69: 250-263.

[19] W Li, J Zhao, W Chen, et al. Three-layer coordinated control of the hybrid operation of static var compensator and static synchronous compensator. *IET Gener. Transm. Dis*., 2016, 10(9): 2185-2193.

[20] L Wang, C S Lam, M C Wong. Multi-functional hybrid structure of SVC and capacitive grid connected inverter (SVC//CGCI) for active power injection and non-active power compensation. *IEEE Trans. Ind. Electron*., 2018, 66(3): 1660-1670.

[21] S Rahmani, A Hamadi, N Mendalek, et al. A new control technique for three-phase shunt hybrid power filter. *IEEE Trans. Ind. Electron*., 2009, 56(8): 2904-2915.

[22] S B Karanki, N Geddada, M K Mishra, et al. A DSTATCOM topology with reduced DC-link voltage rating for load compensation with nonstiff source. *IEEE Trans. Power Electron*., 2012, 27(3): 1201-1211.

[23] S Rahmani, A Hamadi, K Al-Haddad. A Lyapunov-function-based control for a three-phase shunt hybrid active filter. *IEEE Trans. Ind. Electron*., 2011, 59(3): 1418-1429.

[24] F Jiang, X Peng, C Tu, et al. An improved hybrid parallel compensator for enhancing PV power transfer capability. *IEEE Trans. Ind. Electron*., 2022, 69(11): 11132-11143.

[25] S Rahmani, A Hamadi, K Al-Haddad, et al. A combination of shunt hybrid power filter and thyristor-controlled reactor for power quality. *IEEE Trans*. *Ind*. *Electron*., 2014, 61(5): 2152-2164.

[26] L Wang, C S Lam, M C Wong. A hybrid-STATCOM with wide compensation range and low DC-link voltage. *IEEE Trans*. *Ind*. *Electron*., 2016, 63(6): 3333-3343.

[27] Y Xu, F Li. Adaptive PI control of STATCOM for voltage regulation. *IEEE Trans*. *Power Del*., 2014, 29(3): 1002-1011.

[28] B Bai, D Chen, X Wang. Loss calculation of inverter IGBT and design of cooling device. *Transactions of China Electrotechnical Society*, 2013, 28(8): 97-106.

**Xiheng Liang** was born in Jiangxi, China, 1995. He received the B.S. degree from the College of Automation and Electrical Engineering, Linyi University, in 2020. He is currently pursuing the M.S. degree in Electrical Engineering with the Changsha University of Science and Technology, Changsha, China.

His research interests include power electronics converter, distributed generation and power quality control.

**Fei Jiang** (S'15-M'16) received the B.S. and M.S. degrees in Electrical and Information Engineering from Changsha University of Science and Technology, Changsha, China, in 2007 and 2012, respectively, and received the Ph.D. degree in Electrical Engineering from the College of Electrical and Information Engineering, Hunan University, Changsha, China, in 2016.

From 2007 to 2009, he was an Assistant Electrical Engineer at Northwest China Grid Co., Ltd., Xi' an, China. He was a Visiting Scholar with the Chair of Power Electronics, Christian-Albrechts-University of Kiel, Kiel, Germany, in 2019. Currently, he is an Associate Professor with the School of Electronics and Information Engineering, Changsha University of Science and Technology. His current research interests include power electronics converter, distributed generation, and power quality.

**Xing Peng** was born in Sichuan, China, 1996. He received the B.S. degree from the College of Electrical and Information Engineering, Panzhihua University, in 2019. He is currently pursuing the M.S. degree in Electrical Engineering with the Changsha University of Science and Technology, Changsha, China. His research interests include power electronics converter, distributed generation and power quality control.

**Liansong Xiong** (Member, IEEE) was born in Guangyuan, Sichuan, China, in 1986. He received the B.S., M.S., and Ph.D. degrees in Electrical Engineering from Xi'an Jiaotong University (XJTU), Xi'an, China, in 2009, 2012, and 2016, respectively. Since 2014, he has been with the School of E-learning, XJTU, as a part-time Faculty Member. In 2016, he joined the School of Automation, Nanjing Institute of Technology (NJIT), Nanjing, China, introduced in High-Level Academic Talent Plan of NJIT. From 2017 to 2019, he was with the Department of Electrical Engineering, The Hong Kong Polytechnic University (PolyU), Hong Kong, as a Research Associate. He is the first author of 13 articles indexed by SCI and more than 20 articles indexed by Ei. His current research interests include power quality, multilevel converter, renewable energy generation, and stability analysis of converter-dominated power systems. He is a Senior Member of the China Electrotechnical Society, a Member of the China Power Supply Society and the China Society for Electrical Engineering.

**Yongbin Jiang** (Member, IEEE) received the B.S. degree in Electrical Automatization from Jiangsu University, China, in 2012, and the M.S. degree in Instrument Science and Technology and the Ph.D. degree in Electrical Engineering in Xi'an Jiaotong University, Xi'an, China, in 2016 and 2020, respectively. From 2020 to 2022, he worked as the director of Digital Energy Laboratory of the UNISOC (Shanghai) Technologies Co., Ltd., in Shanghai, China. Since 2022, he has been a Research Fellow with Nanyang Technological University, Singapore. His research interests include wireless power transfer, high frequency and high-power density dc/dc converters, signal processing and digital control technology. Dr. Jiang was a recipient of the Best Paper Award of IEEE 10th International Symposium on Power Electronics for Distributed Generation Systems in 2019.

**Samir Gautam** (Member, IEEE) received his B.Sc. in Electrical Engineering (Electronics and Communication) from University of Engineering and Technology (Lahore), Pakistan, and M.E. in Electrical Engineering from Xi'an Jiaotong University, China. He completed his Ph.D. in Electrical Engineering from The University of Sydney, Australia in 2021. His current research interests include grid synchronization, power quality compensators and control of power converters.

**Zhichang Li** was born in Jilin, China, 1984. He received the B.S. degree in Electronic Information Engineering from Jilin Normal University, China, in 2007, and the M.S. in Software Engineering from Nankai University, China, in 2015. He is currently working in Beijing Sgitg-Accenture Information Technology Co., Ltd.